Journal of The Electrochemical Society, **160** (9) D337-D342 (2013)
0013-4651/2013/160(9)/D337/6/$31.00 © The Electrochemical Society

Nucleation of Electrodeposited Lithium Metal: Dendritic Growth and the Effect of Co-Deposited Sodium

Johanna K. Stark,[a,*] Yi Ding,[b] and Paul A. Kohl[a,,z]**

[a]*Georgia Institute of Technology, School of Chemical and Biomolecular Engineering, Atlanta, Georgia 30332-0100, USA*
[b]*U.S. Army RDECOM-TARDEC, AMSRD-TAR-R, MS 159, Warren, Michigan 48397-5000, USA*

Higher energy density batteries are desired, especially for mobile electronic devices. Lithium metal anodes are a possible route to achieving high energy and power density due to their light weight compared to current graphite anodes. However, whisker growth during lithium electrodeposition (i.e. charging) represents a serious safety and efficiency concern for both lithium metal batteries and overcharging of graphite anodes in lithium-ion batteries. The initial morphology of deposited lithium nuclei can have a significant impact on the bulk material deposited. The nucleation of lithium metal from an organic ethylene carbonate: dimethyl carbonate (EC:DMC) and an ionic liquid (trimethylbutylammonium bis(trifluoromethanesulfonyl)imide) electrolyte has been studied. Whisker extrusion and tip-based dendrite growth was observed ex-situ, and confirmed by in-situ optical microscopy experiments. The nucleation of a non-dendritic sodium co-deposit is also discussed. A model based on nuclei geometry is provided which gives insight into the deposition rate at constant overpotential.
 [DOI: 10.1149/2.028309jes]

Manuscript submitted April 5, 2013; revised manuscript received June 4, 2013. Published June 21, 2013.

The lithium metal anode was first used in a primary battery because of the metal's light weight and negative potential. When the anode was tested in a secondary battery, whiskers, also called dendrites, appeared upon recharging were identified as a hazard, leading to the safer graphite intercalation anodes commercialized in secondary batteries today.[1] Lithium whisker growth has been studied, but not fully understood. The mechanism of lithium dendrite growth and mitigation of dendrites is important in realizing a reliable lithium metal anode. Dendrite suppression has also become an important topic in overcharging lithium ion batteries with graphite intercalation anodes. It would be highly desirable to find mechanisms that prevent the formation of dendrites during the unintentional deposition of lithium.

The morphology of electrodeposited and cycled lithium is a function of the electrolyte and electrochemical conditions.[2,3] Lower deposition rates tend to lead to moss-like lithium deposits and delayed dendrite growth. Higher deposition rates result in longer, entangled dendrites.[4,5] At the same time, the resulting higher overpotential at high deposition rates leads to a greater number of individual dendrites, which slows the length growth of individual dendrites. Changing the electrolyte concentration can also have an effect on dendrite growth, although no common trend between electrolytes has been reported.[4,6,7] Depending on the electrochemical system, arguments have been made for higher and lower Li^+ concentrations as a way to decrease dendrite growth; however, such experiments have not lead to elimination of dendrite growth. Given the variety of systems in which dendrites are observed, it is clear that the solid electrolyte interface (SEI) and electrochemical factors have a major role in how dendrites grow, but have not lead to their complete elimination.

Reliable suppression of dendrites has so far been achieved by confining the lithium electrode with a solid ceramic electrolyte, adding selected cations to form and electrostatic shield, and co-depositing metals such as sodium or potassium with lithium. The ceramic electrolyte solves the dendrite problem by providing a physical barrier to dendrite growth. While dendrites are known to grow through separators and even polymers,[2,8] the ceramic electrolyte is an effective physical barrier. Given the large inherent volume change in a lithium metal anode, maintaining contact with the metal electrode during discharge is problematic.[9] Ding et al. showed that adding a small concentration of Cs^+, whose potential is slightly negative of that of lithium, creates an electrostatic shield that results in a dendrite-free lithium deposit.[10] Another metal, such as sodium, can also be co-deposited with lithium to eliminate dendritic growth.[11,12] Although dendrite growth can be suppressed or eliminated, knowledge about the lithium deposition process is important in order to suppress the growth of dendrites under a wide range of conditions. In addition, the recent papers on dendrite-free lithium deposits have coulombic efficiencies less than 100% and often in the 70 to 95% range.[9–12]

Tip growth of dendrites can be electrochemically explained to some extent. It is commonly stated that a rupture in the SEI leaves fresh lithium metal exposed, which is the site for preferential plating leading to the formation of a protrusion.[13] As the dendrite protrudes into the electrolyte different effects can take place such as preferential growth due to the lack of a thick SEI, lower electrolyte resistance, and re-passivation due to SEI formation. These factors affecting dendrite propagation do not result in a constant diameter structure. Dendrites have also been observed to grow parallel to the substrate in coin cells, which indicates an additional driving force.[8,14]

Although theories about growth at the lithium dendrite tip have been proposed, electrochemical dendrite growth originating from the base of the dendrite is more difficult to explain. The area at the intersection of the dendrite base with the substrate (i.e. base-growth) is simply not accessible to the electrolyte, limiting the opportunity for electrodeposition at that location. Base-growth is observed experimentally,[8,15,16] and it appears to occur through a non-electrochemical process, such as by an extrusion process through the SEI.[17] Yamaki et al. present a mechanism where the SEI cracks due to stress from lithium being deposited underneath it. The stress caused by the SEI forces the movement of lithium along defects and grain boundaries. Lithium is forced out of the crack in the SEI, extruding a whisker. Continued growth occurs with lithium depositing on the substrate instead of the protruding whiskers for some time. Lithium then deposits on the tip and kink points of the growing whisker. This mechanism explains the morphology observed but it is hard to explain why, after the SEI rupture, lithium would continue to deposit through the SEI instead of on the freshly deposited lithium at the crack.

The initial form of the metal deposit can be investigated by examining the morphology at different points in the electrodeposition process. When a potential is applied, nuclei populate the surface and begin to grow. The observed current is a direct result of the growing surface area available for deposition. Eq. 1 shows the basic form for the current, where N is the number of nuclei, k is the deposition rate in mol/(cm^{2}s), n is the number of equivalents per mole, and F is Faraday's constant.

$$i = Area_{nuclei} \cdot N \cdot knF \qquad [1]$$

Both N and the $Area_{nuclei}$ are a function of time.[18] The rate at which nuclei appear and their growth geometry determine the overall current. Depending on the applied potential, nucleation will occur immediately (instantaneous nucleation) or progressively over time. The instantaneous and progressive nucleation can be represented as

*Electrochemical Society Student Member.
**Electrochemical Society Fellow.
zE-mail: kohl@gatech.edu

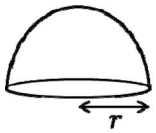

$$i = \left(\frac{2nF\pi M^2}{3\rho^2}\right) \cdot AN_0 t \cdot k^3 \cdot t^2$$

Figure 1. Figure and equation for hemispheric nuclei growth without overlap.

Eqs. 2 and 3 respectively, where N_0 is the total number of nuclei, and A is a nucleation rate.[18]

$$N = N_0 \quad \text{Instantaneous} \qquad [2]$$

$$N = AN_0 t \quad \text{Progressive} \qquad [3]$$

The second factor that contributes to the observed current is the nuclei geometry. This dictates how the area will change with time. If we assume that a nuclei begins with a single atom and grows uniformly outward, a hemispheric shape arises. Fig. 1 illustrates this shape and the resulting equation for the current. The equation predicts a cubic relationship between current and time for short times prior overlap of the nuclei.[18,19] An extension of the model into the time period where nuclei overlap occurs is shown in Fig. 2. The current levels off because the area no longer increases with time once nuclei grow together or when diffusion layers overlap. More complex models that take diffusion into account also exist.[19–23]

In this study, the geometric model was used as a basis analysis of the current in order to gain insight into the appearance and subsequent growth of nuclei, as well as how and when this leads to a dendritic growth. We also present data on lithium/sodium codeposition and how this electrolyte mitigates dendritic growth.[24] Lithium whiskers are observed in lithium electrodeposition as well as overcharging of lithium ion cells.[25] They have been characterized by Liu et al as single crystal but the implications of this discovery have not been discussed. In this work, we describe how lithium dendrite development is based on accelerated growth on specific crystal faces. We suggest a mechanism for sodium as a means of halting dendritic growth supported by optical and electron microcopy, as well as secondary ion mass spectrometry (SIMS) observations.

Experimental

Ethylmethylimidazolium chloride (EMI^+Cl^-, 97%, Acros) and aluminum chloride (anhydrous, Fluka) were used as-received. The initial ionic liquid was made by slowly mixing EMI^+Cl^- and $AlCl_3$ in a 55:45 molar ratio until only a clear liquid remained. The liquid was dried under vacuum for 8 h before adding 100% excess of a metal chloride, either NaCl or LiCl depending on the desired electrolyte.[24,26–28] In order to achieve reversible plating/dissolution of the metal, 0.5 wt% of $SOCl_2$ was added to each melt.

Trimethylbutylammonium bis(triflouromethanesulfonyl)imide (N_{1114}-Tf_2N, 99%, Iolitec) and lithium bis(triflouromethanesulfonyl)imide ($LiTf_2N$, 99%, Wako) were used as-received. Sodium bis(triflouromethanesulfonyl)imide ($NaTf_2N$) was synthesized by the reaction of triflouromethanesulfonylimide (HTf_2N, Wako) with a 1M NaOH solution until the solution was pH neutral. The solution was heated to 60°C and dried under vacuum for 10 h to remove water. Electrolytes were made by dissolving the appropriate amount of metal Tf_2N salt in N_{1114}-Tf_2N followed by drying for several hours before use.

The traditional organic electrolyte was mixed from a 1:1 volume ratio of ethylene carbonate (EC, anhydrous, 99%, Sigma-Aldrich) and dimethyl carbonate (DMC, anhydrous, ≥99%, Sigma-Aldrich) without further purification. Lithium hexafluorophosphate (≥99.99%, Aldrich) was added to make a 1 M lithium electrolyte.

In order to observe dendrites in-situ, an optical cell was constructed between two glass slides. The cell was assembled in an argon glove box by inserting a stainless steel working electrode and a lithium counter/reference electrode into a rubber gasket, which was then pressed between glass slides and held with clips. A syringe was used to fill the cell with electrolyte. The cell was sufficiently air-tight for short-term experiments.

Time of flight secondary ion mass spectroscopy (ToF-SIMS) was used to investigate the elemental distribution of the deposited samples. Lithium or sodium metal was deposited on 316 stainless steel and transferred to the ToF-SIMS. The samples were analyzed with an ION-TOF5 SIMS using bismuth as the primary ion. The analysis area was 20 × 20 μm.

Results and Discussion

The initial stages of lithium growth form the basis for the buildup of a bulk lithium deposit, as would be used in a lithium metal battery anode. Samples were examined by scanning electron microscopy (SEM) after different deposition times using the organic electrolyte. A stainless steel foil electrode was polarized to −150 mV vs. Li/Li^+ in a 1 M $LiPF_6$ EC:DMC electrolyte for a specific amount of time. A progression of SEM images is shown in Fig. 3.

The nuclei in Fig. 3 have a hemispherical shape and a high contact angle with the stainless steel surface. The same contact angle and nuclei shape was observed when the deposition was carried out on

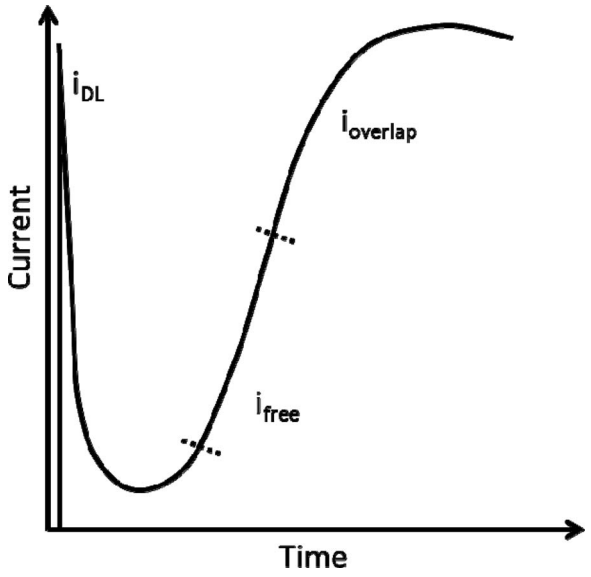

Figure 2. 3D nuclei growth with progressive nucleation and overlap (reproduced with permission).[23]

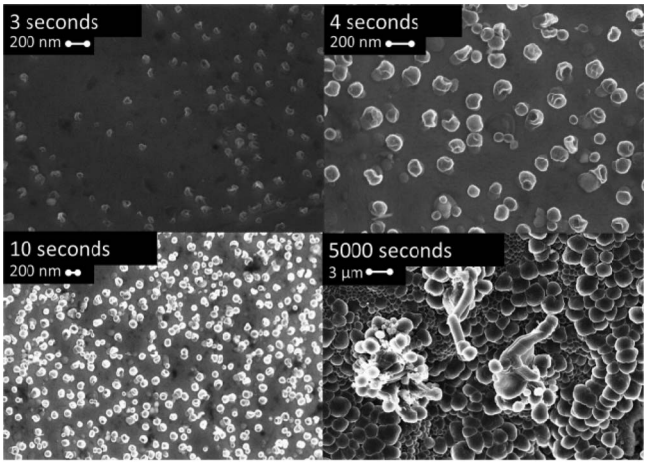

Figure 3. Progression of lithium electrodeposition from 1M$LiPF_6$ EC:DMC. Hemispheric nuclei appear and eventually overlap. At longer times, dendrites appear to extrude from the particle-like layer.

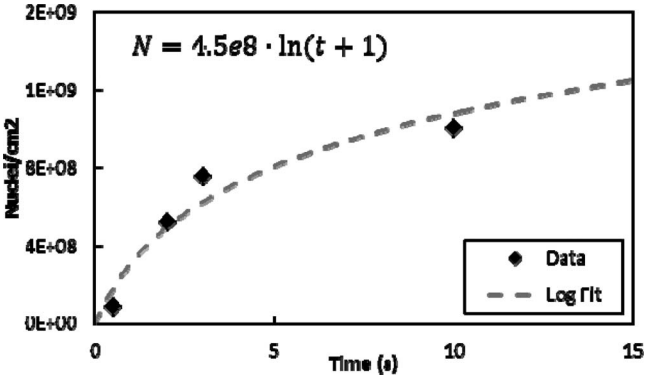

Figure 4. Nuclei density as a function of time in 1M Li^+ EC:DMC.

a section of freshly cleaved lithium foil indicating that the shape of the deposit was not specific to stainless steel. Deposition on a foreign surface can sometimes lead to different morphologies because of a higher overpotential associated with the surface. In this case, the deposit morphologies are likely similar because SEI formation prevents lattice match when plating lithium on a Li substrate, even when the substrate is freshly cleaved. In addition, a cyclic voltammogram of lithium deposition and stripping on stainless steel shows some under-potential deposition (UDP) likely due to lithium intercalation into surface oxides, which may lower the overpotential because the surface becomes more similar.

The nuclei density, *N*, was determined at each time and plotted in Fig. 4. The model presented in Fig. 2 assumes a linear rate of nuclei growth, however, Fig. 4 shows that after an initial sharp increase in sites, the rate levels off. This behavior indicates that there is an overpotential penalty for nucleation and growth of lithium on a non-lithium surface. A foreign surface, such as the stainless steel used here, is expected to provide a barrier to nucleation. The relationship between the number of nuclei and time in Fig. 4 follows a natural log behavior. The growth model in Fig. 2 was adjusted by using a natural log nucleation rate, rather than the linear rate given in Eq. 3.

The experimental current-time plot shown in the inset in Fig. 5 shows the current due to double layer formation, followed by the rise in current to a steady value. The general shape corresponds to the theoretical one outlined in Fig. 2 with several deviations. First, the timescale associated with double-layer formation in Fig. 5 is longer than expected. In our case, the initial current spike also includes lithium intercalation into surface oxides and under-potential deposition (UPD). A small, generally insignificant peak can be seen at 0.5 V vs Li/Li^+ in a cyclic voltammetry scan that contributes to the current at short times. These events delay the nucleation and deposition of

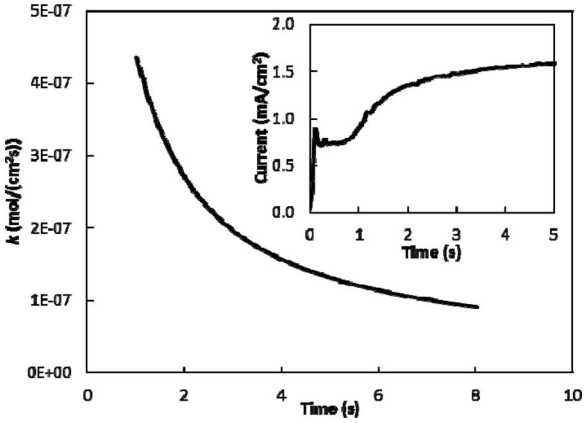

Figure 5. Deposition rate, *k*, solved from the geometric model assuming 3D growth. Inset: Current-time transient for polarization to −150 mV in 1M Li^+ EC:DMC.

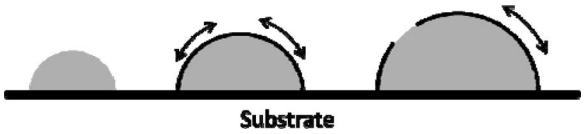

Figure 6. The SEI stretches and breaks as the nuclei grow, resulting in a decreasing deposition rate at constant over-potential.

lithium. A second observation is that the current at long times in Fig. 2 levels off due to the onset of overlapping nuclei and their diffusion layers. When nuclei begin to overlap, the true surface area does not grow as rapidly with time, as when nuclei are forming. The leveling off of the current in Fig. 5 is not due to overlapping nuclei, as shown by sparse distribution of nuclei in Fig. 3.

The deposition rate, *k*, can be solved for by comparing the current-time curve in Fig. 5 to the growth model. The data in Fig. 5 indicates that the growth rate decreases with time, consistent with the inhibiting effect of an SEI layer being formed on the lithium. The lithium/electrolyte interface is influenced by the formation and presence of an SEI layer, however, the model only takes into account the geometry of the system. While the nuclei are able to grow unencumbered at the very beginning, an SEI layer starts to form almost immediately. As each nuclei continues to grow, the SEI layer must be stretched and/or broken to accommodate the growing surface area. This adds additional resistance to nuclei growth, slowing the rate over time, as shown in Fig. 6.

Another observation from this study is that dendrites are not formed at the time of lithium nucleation in the EC:DMC system. The deposit remains mostly dendrite free until 5000 s when dendrites seem to extrude from the deposit. Several dendrites had grooves along their length that further suggest extrusion. Dendrites with a bulged head and narrow trunk were also observed. The latter shape corresponds to the model previously proposed by Yamaki et al. The model is based on an interplay between surface tension and creep strength.[17] When surface tension and creep strength are balanced, a straight-walled whisker is extruded. When surface tension is greater than creep strength, the system is unstable and the dendrites form with a bulbous head, like the ones seen in our experiments. The model predicts that the head would eventually pinch off. Although this was not directly observed, it would be difficult to see this effect since the pinched-off head would have already left the deposit surface.

The same nucleation experiment was conducted in the N_{1114}-Tf_2N electrolyte and yielded very different results. In the EC:DMC electroyle, dendrites did not appear at nucleation and formed much later in the bulk growth process. The same −150 mV over-potential in the ionic liquid system created dendrites immediately after nucleation. Fig. 7 shows SEM images of the lithium deposit from (N_{1114}-Tf_2N)

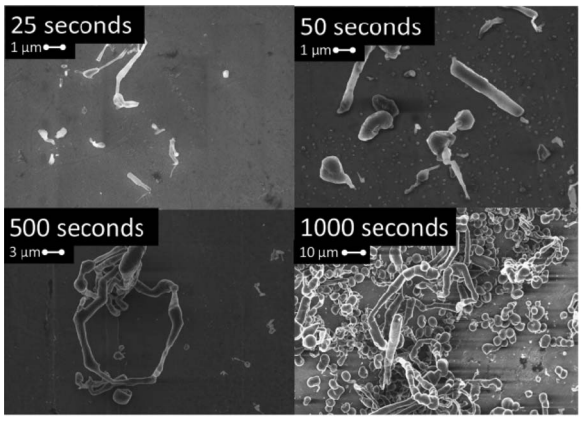

Figure 7. SEM images of deposits from 1M Li^+ N_{1114}-Tf_2N. Nuclei are dendritic immediately upon nucleation. Growth is isolated due to the dendritic shape.

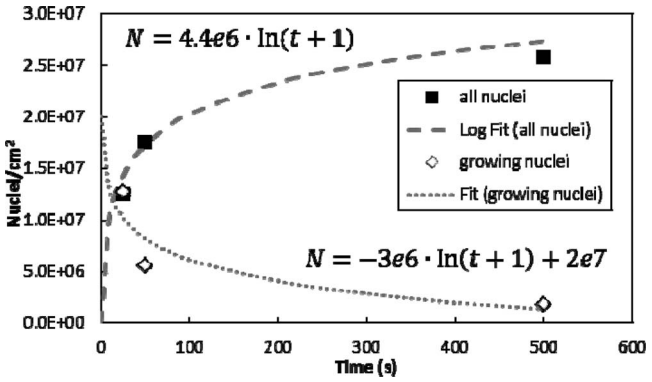

Figure 8. Nuclei appearance as a function of time in 1M Li^+ N_{1114}-Tf_2N.

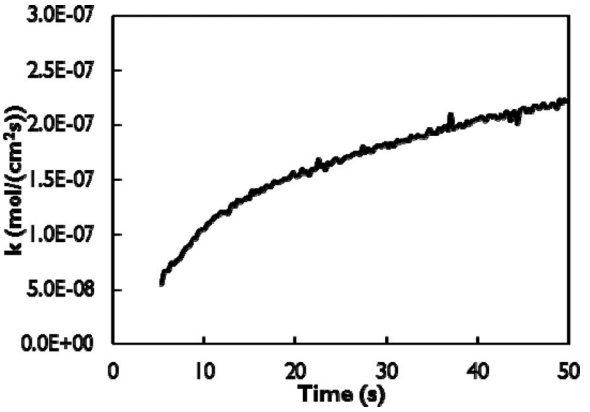

Figure 10. Deposition rate, *k*, solved for by assuming a cylindrical geometry where only the tip is electrochemically active.

at −150 mV. Because of the lower conductivity, deposition in N_{1114}-Tf_2N is slower than that in EC:DMC, resulting in a longer timescale. Small circular nuclei with 100–200 nm diameter initially appear on the surface, but instead of growing with an equally expanding radius, the radius stays almost constant and cylinders form, eventually growing into dendrites. Dendrites do thicken over time, but at a much slower rate than the lengthwise growth.

Tracking the size of the individual nuclei with deposition time in the N_{1114}-Tf_2N electrolyte showed that nuclei growth was not uniform with time. SEM analysis showed that at 50 s, the larger nuclei were micrometer in size, however, a significant number of nanometer sized nuclei were present that did not grow in size. A similar observation was made at 500 s. When only the larger, growing nuclei were counted, a decreasing trend in terms of number of growing nuclei occurred with time, as shown in Fig. 8. The dashed, upper curve in Fig. 8 shows that while the total number of nuclei increases with time, only a small number of nuclei continue to grow and mature to a large size, as shown by the lower, dotted line. Thus the deposition current becomes restricted to a decreasing number of nuclei.

The current-time model used for the EC:DMC case, Fig. 1, is not valid because the hemispheric geometry occurs over a decreasing population. The nuclei geometry observed in the ionic liquid electrolyte was simplified to that of a cylinder with a constant 0.5 μm diameter reflecting the observed results. The current lost to creating the smaller non-growing nuclei was assumed negligible, so the equation used for *N* corresponds to that of the growing nuclei in Fig. 8. An illustration of this modified model is shown in Fig. 9 and the resulting rate *k* in Fig. 10.

If only the decreasing population of nuclei is taken into account from Fig. 8, the growth model can be used to solve for the rate of growth of the large nuclei. The increasing trend for the rate *k* in Fig. 10 indicates that the inhibition behavior of the SEI seen in the EC:DMC electrolyte is not present in the dendritic growth from the ionic liquid electrolyte. The negligible growth on the dendrite sidewalls observed indicates that for the same volume of material, a smaller electrochemically active area is available. This leads to a higher current density and faster growth on those active areas, resulting in whisker growth. There is a timescale for forming the SEI layer on freshly deposited lithium. In the EC:DMC electrolyte, it is possible that the SEI formation time faster than the lithium deposition rate so electrochemically active areas passivate before dendrites can form. In the ionic liquid electrolyte in Fig. 7, the higher current density on the dendrite tips outpaces the SEI formation while other locations are inhibited. This leads to an unstable condition where some nuclei grow faster because the SEI on their electrochemically active areas is thin or unformed. Once a dendrite starts developing an SEI at the tip, growth immediately slows relative to its neighbors. Because of the additional resistance, growth stops altogether soon after as the SEI develops. Meanwhile, the neighboring dendrites see an increased current density due to the decrease in active surface area resulting in even faster growth. In this way, only a few large dendrites and many smaller stunted ones are observed. Because the current density increases with time, the effect of the SEI is mitigated and the deposition rate rises.

It was previously shown that a lithium/sodium co-deposition can mitigate dendrite growth.[24] To further investigate how this occurs, a nucleation-rate study was conducted in a 1 M Li^+/0.1 M Na^+ N_{1114}-Tf_2N electrolyte. Fig. 11 shows SEM images of the stainless steel surface as a function of time. It can be seen that the co-deposition of sodium acts to inhibit dendritic growth from the initial point of deposition, by comparison of Fig. 7 (no sodium) to Fig. 11 (with sodium). Instead of forming cylindrical nuclei (Fig. 7) in the lithium-only electrolyte, the lithium/sodium electrolyte showed round and dimpled nuclei (Fig. 10). The dimples are particularly evident in the 1000 s image of Fig. 11.

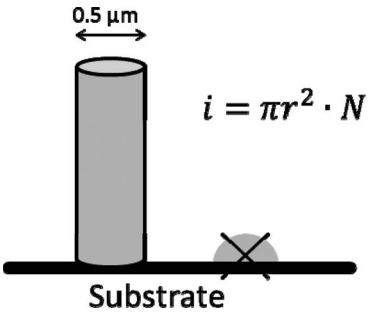

Figure 9. Model based on tip-only growth of dendrites.

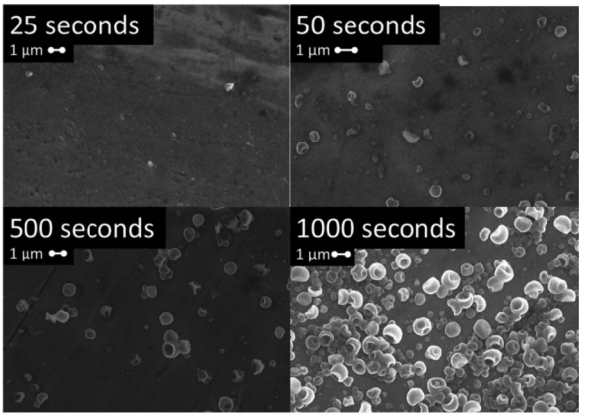

Figure 11. Deposit from 1M Li^+/0.1M Na^+ N_{1114}-Tf_2N appears round and dimpled instead of dendritic.

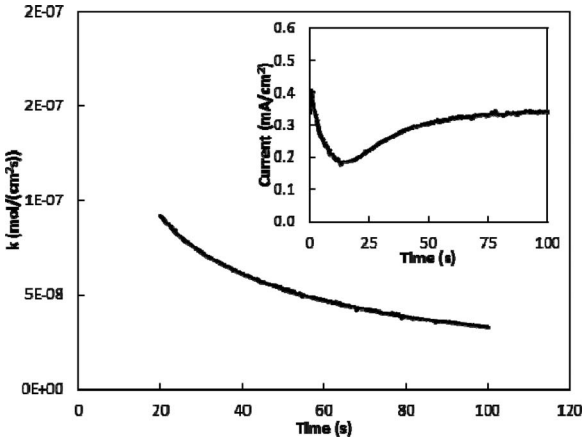

Figure 12. Rate k, for 1M Li^+/0.1M Na^+ N_{1114}-Tf_2N solved for assuming a hemispheric geometry. Inset: Current-time transient for polarization to −150 mV.

As in previous cases discussed here, the number of nuclei over time was fitted to a natural log function instead of a linear fit. The leveling off of the current does not coincide with an overlap of the nuclei. This again points to the inhibiting influence of the SEI layer. If the dimpling were ignored, the geometry of the deposit falls into the hemispherical category and the deposition rate k, can be solved for as in the same manner as the EC:DMC electrolyte. Fig. 12 shows a decreasing trend in k, similar to the EC:DMC electrolyte. As before, this is because stretching and breaking the SEI imposes an additional resistance for the deposition process.

In order for dendrites to grow in the cylindrical manner shown in Fig. 7, the growth rate at the tip must be much higher than the growth rate of the sidewalls. Simple explanations such as the electrolyte resistance being lower at the tip than the base of the dendrite do not explain formation of dendrites because of the variety of experimental setups that produce the whiskers. Given the TEM data presented by Liu et al. confirming the crystillinity of lithium dendrites,[25] the lithium deposition rate is crystal face dependent with some faces being more active for electrdeposition than the other faces. It is possible that the dimpled morphology observed with the co-deposition of sodium results because sodium also deposits on the active lithium face. Sodium would act to inhibit the lithium growth rate because it is a foreign surface and acts to block the progress of the growing dendrite formation. At the same time, lithium continues to deposit in other areas at the normal rate that would otherwise occur because the high current areas are slowed. This would result in a dimpled morphology (Fig. 13).

ToF-SIMS was used to analyze the location of the deposited sodium metal with respect to the lithium nuclei. An element map of a deposit from the 1M Li^+/0.1M Na^+ N_{1114}-Tf_2N electrolyte is shown in Fig. 14. Individual lithium particles are observed on the substrate of the sample, as well as very localized sodium particles. It is clear that sodium was not deposited uniformly on the substrate but rather in very specific areas. This observation supports the theory that sodium was likely deposited on the active face of lithium, thus blocking dendrite growth.

Figure 13. Sodium could block dendrite growth by depositing on electrochemically active lithium faces. Foreign surface effects of lithium and sodium could prevent further deposit in that area while the rest of the nuclei continues to grow resulting in a dimple.

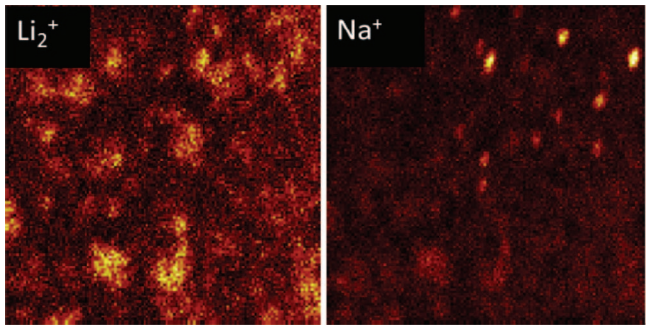

Figure 14. Element map from Tof-SIMS for deposit from a 1M Li^+/0.1M Na^+ N_{1114}-Tf_2N electrolyte.

Ex-situ, SEM images point to the existence of both extruded dendrite growth and tip-based dendrite growth. In-situ observations of dendrite growth were performed to better understand the growth mechanism. Images of single dendrite growth were recorded as a function of time. A cell sandwiched between two glass slides, as described in the experimental section, was used to observe dendrites in an optical microscope. Dendrites grown from EC:DMC and N_{1114}-Tf_2N electrolytes were both on the order of micrometers in size and thus too small to observe in a light microscope. Lithium deposited from the imidazolium chloroaluminate electrolyte produced much larger dendrites, tens of μm in diameter, which could be observed with an optical microscope. Video footage was recorded at 5 mA/cm^2 applied current. Fig. 15 shows frames from two separate dendrites whose growth was observed with time.

Fig. 15A follows a dendrite that developed a kink. Using the kink as a reference point, we can clearly see dendrite growth progressing via the tip of the dendrite. The growth rate at the tip was far greater than the growth from on the sidewalls, suggesting that the crystal face at the tip was significantly more electrochemically active. This cannot be explained by mass transfer effects alone because once the deposit is clear of the lithium at the base, the sidewalls around the tip are in a similar environment as the tip itself. One might expect a widening at the tip due to diffusion, but this does not occur. The fact that the dendrite was straight before and after the kink further supports that the dendrite is crystalline in nature and the kink arose from a defect in the crystal. Fig. 15B shows a different case where a lithium structure spawned a looped dendrite. In the first frame, two loops can be seen coming out of the main lithium structure. In subsequent frames, the loops become larger but no tip was visible to propagate the growth. The most reasonable explanation is that lithium was extruded out from the main structure.

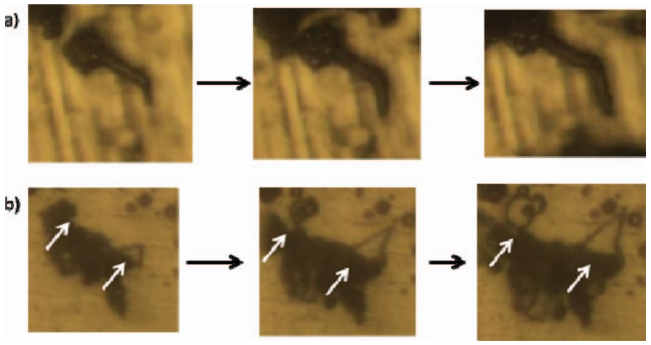

Figure 15. Optical microscope observations of individual dendrite growths in imidazolium chloroaluminate ionic liquid. a) Tip growth shown by a kinked dendrite and b) base growth of two loops by extrusion.

Discussion

We were able to definitively observe both tip-based and extrusion-based dendrite growth in-situ and ex-situ. Tip-based growth is an electrochemical process where the tip is an electrochemically active face that grows at a significantly faster rate than the sidewalls or base. Extrusion-based growth is not a direct electrochemcial event, but rather occurs as a side-effect of pressure buildup as a result of lithium deposition under a strained SEI layer.

Sodium can play a crucial role in suppressing tip-based dendrite growth. When sodium is co-deposited with lithium, the two metals do not form an alloy. Instead, distinct areas of sodium are visible in the ToF-SIMS analysis. Considering the lack of dendrites when these sodium clusters are present, it is believed that lithium dendrites can grow because of increased electrochemical activity on a specific crystal face of lithium. Sodium acts to block the accelerated growth and resulting in a dimpled and dendrite-free morphology. Such a blocking effect could also be the reason why no dendrites are seen in EC:DMC or with certain additives such as HF and VC.[29–31]

No tip-growth dendrites were observed in this set of experiments from EC:DMC while many were observed in N_{1114}-Tf_2N. The SEI formed in these electrolytes is chemically very different. The SEI formed in N_{1114}-Tf_2N consists of mainly LiF,[32] while the EC:DMC system forms a layer of EC decomposition products such as alkoxides.[33] The physical properties of these layers will also likely be very different. It is probable that alkoxides and other additives can have a similar blocking affect as the sodium co-deposit observed here or that the SEI is simply robust enough to suppress the tendency for high-rate dendritic growth. Sodium is advantageous over electrolyte decomposition materials because it can double as active material in the cell. Sodium can be oxidized along with the lithium anode and thus the charge stored is not lost. Sodium can then be re-deposited in the next cycle without material waste whereas fresh electrolyte would have to be decomposed on the new active areas in each cycle.

By using the geometry of the nuclei at short times, it was possible to draw several conclusions about the effect of the SEI on the current-time transient. The SEI provided significant resistance to lithium deposition as seen by examination of the electrochemical rate as determined from the geometric model. Under constant potential, the rate dropped from an initially high value because the SEI imposed additional resistance as it fully formed. In the dendritic case, lithium deposition occurred over a limited active area. The high current density resulted in lithium deposition that outstripped the SEI formation, so an initial increasing rate was observed.

While this work looked at early deposits only, there are consequences for the thicker deposits that might be used in the lithium metal battery. The deposition of contiguous films of metal with excellent coulombic efficiency upon cycling are highly desired but the SEI plays a large role in preventing nuclei from growing together in long-time experiments. Despite non-dendritic results with sodium co-deposition, the SEI film formed on lithium still presents a major hurdle for the lithium-metal anode.

Acknowledgments

The authors gratefully acknowledge the financial support of the US Army, contract US001-0000245070.

References

1. J.-M. Tarascon and M. Armand, *Nature*, **414**, 359 (2001).
2. M. Rosso, T. Gobron, C. Brissot, J.-N. Chazalviel, and S. Lascaud, *Journal of Power Sources*, **97–98**, 804 (2001).
3. L. Gireaud, S. Grugeon, S. Laruelle, B. Yrieix, and J.-M. Tarascon, *Electrochemistry Communications*, **8**, 1639 (2006).
4. K. Nishikawa et al., *Journal of The Electrochemical Society*, **157**, A1212 (2010).
5. C. Brissot, M. Rosso, J.-N. Chazalviel, and S. Lascaud, *Journal of Power Sources*, **81**, 925 (1999).
6. S.-K. Jeong et al., *Electrochemistry Communications*, **10**, 635 (2008).
7. K. Nishikawa, T. Mori, T. Nishida, Y. Fukunaka, and M. Rosso, *Journal of Electroanalytical Chemistry*, **661**, 84 (2011).
8. M. Dollé, L. Sannier, B. Beaudoin, M. Trentin, and J.-M. Tarascon, *Electrochemical and Solid-State Letters*, **5**, A286 (2002).
9. F. Sagane, R. Shimokawa, H. Sano, H. Sakaebe, and Y. Iriyama, *Journal of Power Sources*, **225**, 245 (2013).
10. F. Ding et al., *Journal of the American Chemical Society* (2013).
11. K. P. Doyle, C. M. Lang, K. Kim, and P. A. Kohl, *Journal of The Electrochemical Society*, **153**, A1353 (2006).
12. J. K. Stark, Y. Ding, and P. A. Kohl, *Journal of The Electrochemical Society*, **158**, A1100 (2011).
13. D. Aurbach, E. Zinigrad, Y. Cohen, and H. Teller, *Solid State Ionics*, **148**, 405 (2002).
14. H. Ota, X. Wang, and E. Yasukawa, *Journal of The Electrochemical Society*, **151**, A427 (2004).
15. P. C. Howlett, D. R. MacFarlane, and A. F. Hollenkamp, *Journal of Power Sources*, **114**, 277 (2003).
16. O. Crowther and A. C. West, *Journal of The Electrochemical Society*, **155**, A806 (2008).
17. J. Yamaki, S. Tobishima, K. Hayashi, Y. Nemoto, and M. Arakawa, *Journal of Power Sources*, **74**, 219 (1998).
18. M. Paunovic and M. Schlesinger, *Fundamentals of Electrochemical Deposition*, John Wiley & Sons, Inc., New York, (1998).
19. B. Scharifker and G. Hills, *Electrochimica Acta*, **28**, 879 (1983).
20. R. D. Armstrong, M. Fleischmann, and H. R. Thirsk, *Journal of Electroanalytical Chemistry*, **11**, 208 (1966).
21. D. J. Astley, J. a. Harrison, and H. R. Thirsk, *Journal of Electroanalytical Chemistry and Interfacial Electrochemistry*, **19**, 325 (1968).
22. M. Fleischmann and H. R. Thirsk, *Journal of The Electrochemical Society*, **110**, 688 (1963).
23. H. Bort, K. Juttner, W. J. Lorenz, G. Staikov, and E. Budevski, *Electrochimica Acta*, **28**, 985 (1983).
24. J. K. Stark, Y. Ding, and P. A. Kohl, *Journal of The Electrochemical Society*, **158**, A1100 (2011).
25. X. H. Liu et al., *Applied Physics Letters*, **98**, 183107 (2011).
26. T. L. Riechel and J. S. Wilkes, *Journal of The Electrochemical Society*, **139**, 977 (1992).
27. C. Scordilis-kelley and R. T. Carlin, *Journal of The Electrochemical Society*, **141**, 873 (1994).
28. G. E. Gray, P. A. Kohl, and J. Winnick, *Journal of The Electrochemical Society*, **142**, 3636 (1995).
29. S. Shiraishi, K. Kanamura, and Z. Takehara, *Journal of Applied Electrochemistry*, **29**, 869 (1999).
30. K. Kanamura, S. Shiraishi, and Z. Takehara, *Journal of The Electrochemical Society*, **143**, 2187 (1996).
31. H. Ota et al., *Journal of The Electrochemical Society*, **151**, A1778 (2004).
32. J. K. Stark, Y. Ding, and P. A. Kohl, *The Journal of Physical Chemistry C*, **117**, 4980 (2013).
33. K. Xu et al., *The Journal of Physical Chemistry B*, **110**, 7708 (2006).